Structure and dynamics of water confined in nanoporous carbon

Yuzi He,[1,2] Ken-ichi Nomura,[1,3] Rajiv K. Kalia,[1,2,3,4] Aiichiro Nakano,[1,2,3,4,5] and Priya Vashishta[1,2,3,4]

[1]*Collaboratory for Advanced Computing and Simulations, University of Southern California, Los Angeles, California 90089-0241, USA*

[2]*Department of Physics & Astronomy, University of Southern California, Los Angeles, California 90089-0241, USA*

[3]*Department of Materials Science and Chemical Engineering, University of Southern California, Los Angeles, California 90089-0241, USA*

[4]*Department of Computer Science, University of Southern California, Los Angeles, California 90089-0241, USA*

[5]*Department of Biological Science, University of Southern California, Los Angeles, California 90089-0241, USA*

(Received 22 May 2018; revised manuscript received 10 August 2018; published 29 November 2018)

We study the structure and dynamics of water confined in a nanoporous graphitic carbon structure using molecular-dynamics (MD) simulations. The carbon structure is generated by a reactive MD simulation of oxidation of a silicon carbide nanoparticle. We embed water molecules in the nanopores and study structural and dynamical properties of nanoconfined water as a function of temperature. MD simulation results indicate the presence of high-density water (HDW) and low-density water. Radial distribution functions and spatial density functions indicate that the second solvation shell of the HDW is broken. We calculate the self-diffusion coefficient of confined water molecules as a function of temperature and find a significant decrease in the diffusion of water molecules around $T = 190$ K. The cage correlation function $c(t)$ of confined water molecules at $T = 200$ K exhibits stretched exponential decay, $c(t) = \exp[-(t/\tau)^{\beta}]$, with $\beta = 0.43$, which matches exactly with the theoretical prediction $\beta = 3/7$. Furthermore, the self-intermediate scattering function at $T = 200$ K indicates differences in small-scale and large-scale dynamics of water molecules.

DOI: 10.1103/PhysRevMaterials.2.115605

I. INTRODUCTION

Nanoporous carbon is a promising material for many technological applications. Porous carbon is known to be a good candidate for electrodes in lithium-air batteries [1]. A recent study indicates that porous carbon is highly compressible and superelastic [2]. This unique mechanical property has potential applications in composites. It has been reported that carbon-based material could be used to make aerogel muscles [3]. Nanoporous carbon has good capacity for hydrogen storage because it can be synthesized with large surface area [4]. Efforts have been made to use nanoporous carbon as a catalyst. For example, sulfonated nanoporous carbon can be used to convert biomass to fuel and other chemical products [5]. Nitrogen-doped nanoporous carbon has applications in heterogeneous hydrogenation and oxidation, either as a catalyst or catalyst supporter [6].

In many of these applications, nanoporous carbon is in aqueous environments. We have performed molecular-dynamics (MD) simulations of water molecules confined in nanoporous carbon. The physical properties of confined water molecules are quite different from bulk water. Experiments and simulations of confined water have been reported recently. A Raman spectroscopy study shows that the melting temperature of water confined in isolated carbon nanotubes (CNTs) is significantly higher than 0 °C [7]. These experiments indicate that the freezing-transition temperature is highly sensitive to the diameter of the CNTs. In a related study, it is observed that water molecules can form various ice nanotubes in CNTs and these structures are very different from the bulk ice phases [8]. The transitions between these structures can be both first order and continuous [8].

A recent MD simulation [9] of water molecules confined in nanoporous silica shows that there exists a mixture of high-density water (HDW) and low-density water (LDW) in the "no man's land" of water's phase diagram [10]. The dynamical behavior of water molecules changes dramatically under confinement. Shekhar *et al.* [9] have analyzed the dynamics of water confined in nanoporous silica using the cage correlation function. This function reflects changes in the nearest-neighbor configuration of a molecule and how the mean-square displacement (MSD) of the molecule changes with time. Shekhar *et al.* found diffusive regimes separated by plateaus in the MSDs of confined water molecules. A plateau in an MSD indicates that a water molecule is trapped in a cage formed by its nearest neighbors. The water molecule rattles around in the cage until the cage is broken, allowing the molecule to diffuse. Shekhar *et al.* report that the cage correlation function, c(t), of water molecules exhibits stretched exponential behavior, namely $c(t) = \exp[-(t/\tau)^{\beta}]$. They find $\beta = d/(d+2) = 0.6$, where $d = 3$ is the dimensionality of the system. This value of β agrees with an exact theoretical result [11] for anomalous diffusion under confinement if the molecules have no long-range interaction. In another MD simulation [12] study of supercooled water confined in SiC nanotubes, the cage correlation function is again found to decay as $\exp[-(t/\tau)^{\beta}]$ and $\beta = d^*/(d^*+2) = 3/7$, where $d^* = fd = d/2$ due to long-range Coulomb interaction [13]. This is also in agreement with the exact asymptotic behavior of $c(t)$ [14].

In the simulations reported here, we study both structural and dynamical properties of water confined in nanoporous carbon generated by oxidation of a silicon carbide nanoparticle using reactive molecular-dynamics (RMD) simulation

[15]. Our simulations show that water confined in nanopores of nanoporous carbon is a mixture of HDW and LDW at $T < 232$ K [10]. We find that the density difference between LDW and HDW is almost 0.3 g/cc and that the structures of LDW and HDW are significantly different. Unlike the complete second hydration shell of LDW, the second hydration shell of HDW is broken. These structural differences have been observed in neutron-diffraction experiments and empirical potential structure refinement [16]. As for the dynamics of nanoconfined water, we find that freezing starts around $T = 190$ K. Above freezing, at $T = 200$ and 250 K, the cage correlation functions of water molecules decay as $c(t) = \exp[-(t/\tau)^{\beta}]$, where β is again very close to the theoretical prediction $\beta = 3/7$. We have also calculated the self-intermediate scattering function (ISF), $f(k, t)$, of water molecules at 200 K for different wave vectors. and fitted the data to stretched exponential functions $C(t) = \exp\{-[t/\tau(k)]^{\beta(k)}\}$. We find that $\beta(k)$ and $\tau(k)$ decrease as the wave vector k increases. The latter decreases as k^{-2} for small k and much more sharply for large k. This k dependence shows dynamical differences between small- and large-scale motion of water molecules confined in nanoporous carbon.

II. METHODOLOGY

A. Preparation of nanoporous carbon

Nanoporous carbon is computationally synthesized with RMD simulations [17,18]. The RMD approach is based on reactive force fields (ReaxFF), which allow bond breaking, bond formation, and charge transfer between atoms. In ReaxFF, the interaction energy between atoms has the following functional form:

$$E_{\text{system}} = E_{\text{bond}} + E_{\text{over}} + E_{\text{under}} + E_{\text{val}} + E_{\text{pen}} + E_{\text{tors}} + E_{\text{conj}} + E_{\text{vdWaals}} + E_{\text{Coulomb}},$$

where E_{bond} is the bond energy; E_{over} and E_{under} are the energies of over-/undercoordinated atoms; E_{val} is the valence angle term; E_{pen} is the penalty energy for two double bonds sharing a single atom; E_{tors} is the energy which depends on torsion angles; E_{conj} describes the energy of conjugated systems like benzene; E_{vdWaals} is the nonbonded van der Waals energy; and E_{Coulomb} describes the long-ranged Coulomb interaction. The parameters in the force field are fitted to quantum-mechanical calculations based on density-functional theory. The expression for each term and the parameters for SiC are given in Ref. [19].

We have used this force field to study oxidation of a SiC nanoparticle (n-SiC). In the simulation, a SiC nanoparticle is oxidized at $T = 2800$ K. Initially, the oxidation process produces a silica shell around the unreacted SiC core. The silica-shell thickness exhibits a transition from an initial fast oxide growth limited by the reaction rate to slow growth limited by the diffusion of reactants to the oxide/SiC interface. Since silicon atoms react readily with oxygen atoms to form SiO_2, the remaining carbon atoms form C–C covalent bonds. The resulting nanoporous carbon structure is shown in Fig. 1(a). The density of the nanoporous carbon (n-C) structure is 0.5 g/cm^3. Most of the carbon atoms in n-C form six-membered rings but some of them form five- and seven-membered rings, which are considered defects. We have analyzed the pore-size distribution using voxels of length 3.1 Å, which corresponds to the size of a water molecule at normal density (1.0 g/cc). The pore size ranges between 1.6 and 5.6 nm^3 and the largest pore has ∼200 water molecules. We performed only one RMD simulation of oxidation of n-SiC and therefore we have a single realization of n-C.

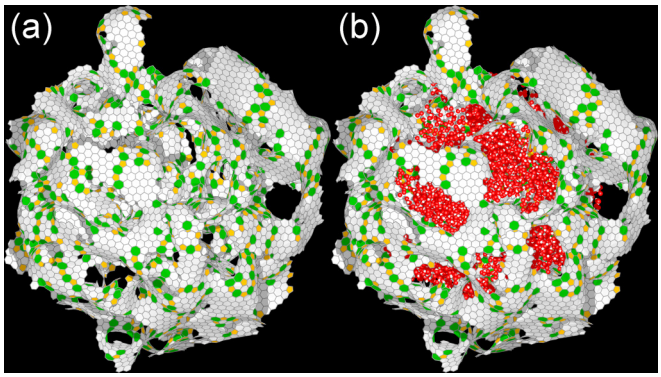

FIG. 1. (a) The nanoporous carbon structure. Carbon atoms form five-, six-, and seven-membered rings which are color coded by yellow, white, and green, respectively. The analysis of pore-size distribution indicates that the largest pore has a radius of gyration $Rg = 7.76$ Å. (b) The nanoporous carbon structure with embedded water molecules. Red spheres represent oxygen atoms and white spheres are hydrogen atoms. Only water molecules inside the carbon structure are shown here.

B. MD simulation of confined water

After the synthesis of nanoporous carbon structure, we switched the C-C force field from ReaxFF to adaptive intermolecular reactive bond order (AIREBO) [20] and ran an MD simulation for 1.0 ns at $T = 300$ K with a time step of 1.0 fs. We estimated the volume of the carbon structure using a convex hull and found that the volume change was less than 3%. Over 98% of carbon atoms had the same nearest neighbors as in ReaxFF, which shows that the carbon structure is well described by the AIREBO force field.

Water molecules are embedded in the nanoporous carbon structure enclosed in a rectangular simulation box. The box is divided into 38 × 44 × 39 voxels of length 3.1 Å. We embed one water molecule in each empty voxel, making sure that no H_2O molecule is closer than 3.50 Å from the nearest carbon atom. Our system contains 16,996 carbon atoms and 55,935 water molecules. We use TIP4P/2005 force field [21] for water, which can describe thermodynamic properties and the phase diagram of condensed phases over a temperature range from 123 to 573 K and pressures up to 40, 000 bar. Water-carbon interaction is described by a Lennard-Jones (LJ) potential. The LJ parameters $\sigma_{\text{co}} = 0.319$ nm and $\varepsilon_{\text{co}} = 0.339$ kJ/mol [22] were fitted specifically for TIP4P/2005 water and graphene. The contact-angle calculation for the force-field development is described in Ref. [22]. They use a new method to make an accurate estimate of the contact angle of water droplets on graphene and validate the force field by experiment [23]. The resulting contact angle $\theta = 90^{\circ}$, which is generally the accepted experimental value [23]. We include

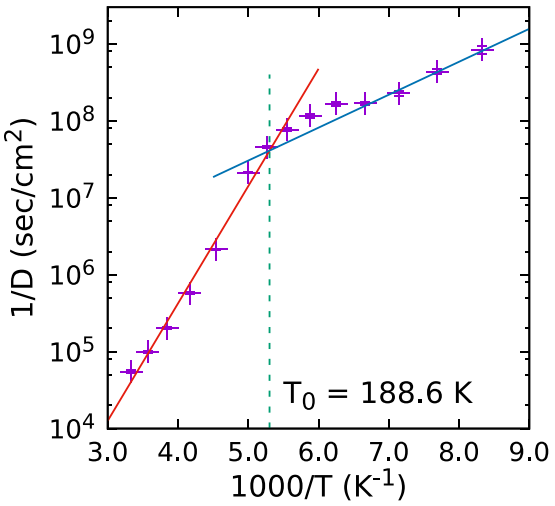

FIG. 2. $1/D$ vs $1/T$ plot shows two distinct regions. The transition temperature is the intersection of the two straight lines fitted to simulation data. Below the transition temperature, the self-diffusion constant is two orders of magnitude smaller than the room-temperature value, which indicates that water is nearly frozen. Above the transition temperature, the self-diffusion constant increases exponentially.

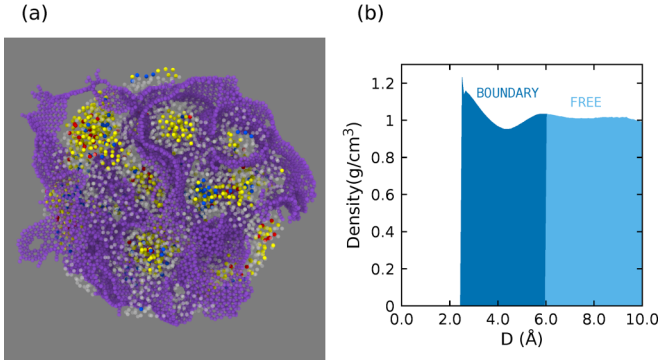

FIG. 3. (a) Snapshot shows water molecules in nanoporous carbon. Here only oxygen atoms of water molecules are shown. Blue and red circles represent HDW (1.1–1.3 g/cc) and LDW (0.7–0.9 g/cc) molecules, respectively. Yellow circles are water molecules at normal density (0.9–1.1 g/cc). Purple circles are carbon atoms and white semitransparent circles are water molecules in the buffer region (within 6.0 Å from carbon atoms). HDW and LDW molecules tend to form clusters in nanopores [34]. (b) Density profile at $T = 200$ K. The average density of water is greater than 1.1 g/cc near nanopore surfaces. The density decreases to 0.95 g/cc as the distance from nanopore surfaces increases. The average density of water is close to 1.0 g/cc at distances larger than 6.0 Å from pore surfaces.

long-range Coulomb interaction and apply periodic boundary conditions in the x, y, and z directions. First, we equilibrate the system in the isothermal-isobaric (NPT) ensemble ($P =$ 1.0 bar, $T = 300$ K) and then switch to the canonical (NVT) ensemble. Simulations are performed at various temperature between $T = 100$ and 300 K using a heat bath to control the temperature of only the nanoporous carbon structure [24]. We use a time step $dt = 1.0$ fs. Systems are first thermalized for 1.0 ns and then structural properties are calculated over the next 1.0 ns. Cage correlation and self-intermediate scattering functions are calculated for at least 16 ns.

We have estimated the amount of water adsorbed in n-C by counting the total number of water molecules inside a sphere of radius 60 Å centered at the center of mass of carbon atoms. There are 2.3×10^4 water molecules in that sphere. Since the MD box size remains the same at different temperatures, the number of adsorbed water molecules shows no significant change.

III. RESULTS AND DISCUSSION

We calculated the mean-square displacement of confined water molecules that were at least 5.0 Å away from carbon atoms. The temperature dependence of the self-diffusion coefficient, namely $1/D$ vs $1/T$ data, of those molecules is shown on a log-linear plot in Fig. 2. For comparison, the temperature dependence of bulk water is included in the Supplemental Material [25]. There are two distinct regions in Fig. 2, indicating a transition at $T_0 \approx 190$ K. The self-diffusion coefficient of water is smaller than 10^{-7} cm^2/s below the transition temperature, and increases as $D \sim \exp(-E_0/k_B T)$ above T_0. The linear fits below and above T_0 give an impression that there exists a transition region. We examined the structure of water in that temperature range and found none of the characteristics of the no man's land. Ultrafast x-ray probe experiment indicates an increase in structural ordering upon supercooling to ~229 K [26]. We do not observe such an ordering in the transition region.

A. Structure

The phase diagram of water consists of several regions: liquid phase above 273 K and supercooled water in the temperature range $232\,\text{K} < T < 273\,\text{K}$. Below 160 K, water forms low-density amorphous (LDA) and high-density amorphous (HDA) ice. Between $160\,\text{K} < T < 232\,\text{K}$ lies a metastable region called the no man's land [10]. The LDA and HDA ice melt into low-density water and high-density water [9].

We calculated the density of water molecules at $T = 200$ K using the Voronoi cell construction to examine the structure of water confined in nanoporous carbon. The inverse of the Voronoi cell volume around each H_2O molecule gives the local density of H_2O at the molecular level. We find 18% of water molecules are HDW (density > 1.1 g/cc) and 7% are LDW (density < 0.9 g/cc). The remaining water molecules have normal density (0.9–1.1 g/cc). Nanoconfined HDW and LDW molecules form clusters, see Fig. 3(a).

A previous MD study of the structure and dynamics of water confined in nanoporous amorphous silica [9] indicated approximately equal number of LDW and HDW in the nanoporous structure. Thus, it appears that the densities of LDW and HDW depend on the confining medium and the internal structures of pores. The nanoporous carbon structure is hydrophobic, whereas the nanoporous silica structure is hydrophilic. These characteristics of confining materials affect the relative densities of LDW, HDW, and normal water. Furthermore, the temperature of the system can also change the density distribution of LDW and HDW. Above a certain temperature, the distinction between LDW and HDW disappears even in the case of bulk water.

We examined the density profile of water near the pore surfaces. The distance is calculated using the nearest carbon atom from a specific water molecule and the density from the Voronoi cell volume. Figure 3(b) shows the density as a function of the distance between water molecules and carbon atoms in the so-called "boundary" and "free" regions. In the free region, the density of water is 1.0 g/cc. In the boundary region, the density of water is affected by hydrophobic interaction and is 10% higher than the average density. As the distance increases, the density decreases to 0.95 g/cc and then increases again to 1.0 g/cc. For water molecules at least 6.0 Å away from carbon atoms, the average density is close to 1.0 g/cc. The minimum density is observed at $d = 4.4$ Å, and it is due to the interaction between water molecules. Similar results have been reported [27] for the density profile of water confined in Mobil Composition of Matter No. 41 (MCM-41). There are some differences arising from the fact that MCM-41 is hydrophilic and nanoporous carbon is hydrophobic and therefore we only observe an increase in the local density closer to the pore surfaces. Results in Fig. 3(b) can be attributed to the packing effect due to hydrophobicity of n-C [28].

We cool the system to further examine the local structure of LDW and HDW in amorphous states. Previous studies have shown that freezing of water is suppressed under strong confinement [7]. We calculate the radial distribution function (RDF) and spatial density function (SDF) at 100 K. LDW and HDW molecules are chosen at least 6.0 Å from carbon atoms to ensure that first and second solvation shells are captured. We calculate the density of water using Voronoi cells. The LDW density is chosen between 0.7 and 0.9 g/cc and the HDW between 1.1 and 1.3 g/cc. The RDFs of LDW and HDW at $T = 100$ K are shown in Fig. 4. The first peak of HDW appears at a slightly smaller distance than the one in LDW. The number of nearest neighbors is still four for both LDW and HDW. The RDF of LDW has a well-defined second peak, whereas the RDF of HDW has a broad second maximum.

We have also calculated the SDF of HDW and LDW from MD trajectories. Unlike RDF, SDF shows anisotropic distribution of density. We choose the origin at an oxygen atom and the x axis is taken along the line joining the two hydrogen atoms. The z axis starts from the oxygen atom and passes through the midpoint of the two hydrogen atoms. The y axis is chosen normal to both x and z axes. Note that a water molecule in the TIP4P/2005 model is a rigid, symmetric body. Therefore, these axes are valid for water molecules in different positions and orientations. The SDF plots are generated using the positions of oxygen atoms and by smearing Gaussian spheres of diameter 1.0 Å around oxygen atoms. In Figs. 4(b) and 4(c), we plot isosurfaces of SDFs for HDW and LDW. We choose the second maxima in RDFs to show second hydration shells of both HDW and LDW. The SDF of LDW has two ring structures, whereas the isosurface of SDF for HDW is smooth and has no anisotropic features. This indicates that the second hydration shell of LDW is complete and the second solvation shell of HDW is not. This is consistent with the simulations of nanoconfined water in nanoporous silica [9] and furthermore, the neutron-scattering experiment by Soper and Ricci corroborates this result [16].

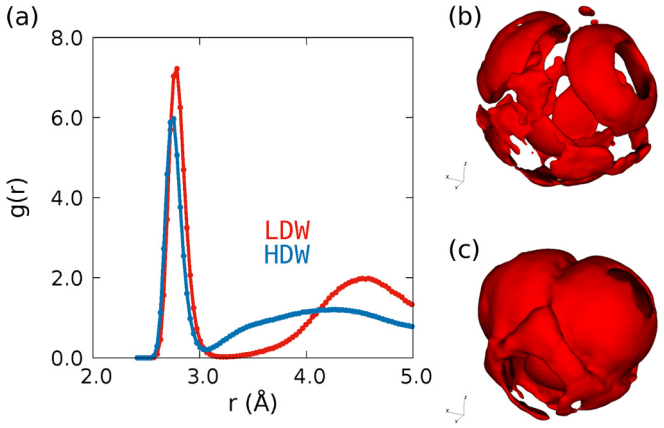

FIG. 4. (a) RDFs at $T = 100$ K reveal that HDW does not have a well-defined second maximum. (b), (c) Spatial density functions of LDW and HDW, respectively, at $T = 100$ K. The SDF is plotted as an isosurface with spatial density corresponding to the height of the second maximum in RDF. There are two symmetric ring structures in the upper region of the SDF for LDW. In contrast, the SDF of HDW is smooth with no spatial heterogeneity, which indicates that the second solvation shell is broken [29].

B. Dynamics

MSDs of nanoconfined water molecules as a function of time display diffusive regimes separated by plateaus below $T = 250$ K. A plateau in the MSD of a water molecule indicates that the molecule is trapped in a cage formed by its nearest neighbors. The water molecule rattles around in the cage until the cage is broken, allowing the molecule to diffuse.

We have calculated the cage correlation function (CCF), $C(t)$, at $T = 200$ and 250 K using the formula

$$c(t) = \frac{\left\langle \sum_i l_i(t) \cdot l_i(0) \right\rangle}{\left\langle \sum_i l_i(0)^2 \right\rangle}, \tag{1}$$

where $l_i(t)$ are the nearest neighbors (within a cutoff distance of 3.14 Å, corresponding to the first minimum in the RDF) of particle number i at time t [9,29]. $l_i(t)[j] = 1$ when j is a nearest neighbor of i at time t, and $l_i(t)[j] = 0$ otherwise. The CCF provides a quantitative analysis of the dynamics of water confined in nanoporous carbon. It describes changes in the nearest-neighbor configurations of particles. By definition, $c(t) = 1$ at $t = 0$. When the nearest neighbor of all the particles in a group has changed completely, $c(t) = 0$.

We find $c(t)$ can be fitted to a stretched exponential function,

$$c(t) = \exp(-(t/\tau)^{\beta}), \tag{2}$$

at $T = 200$ K, see Fig. 5. The exponent β is found to be 0.43, and $\tau = 1.85$ ns. Note that we only fit the tail of $c(t)$ where $c(t) < 1/e$. In our calculation, it takes 2.64 ns for $c(t)$ to decay from 1 to $1/e$. We have also calculated the cage correlation function at $T = 250$ K and we again observe stretched exponential relaxation with an exponent $\beta = 0.40$, which is close to the theoretical prediction, $\beta = 3/7$.

Shekhar *et al.* [9] also find stretched exponential decay for the cage correlation function of water molecules confined in

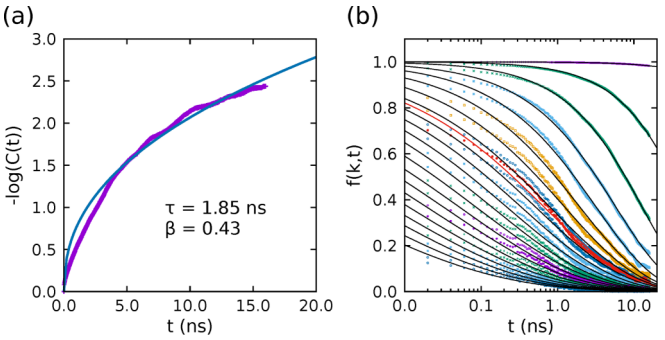

FIG. 5. (a) $-\mathrm{Log}[C(t)]$ vs time. The calculated values (purple dots) are fitted to the blue line. (b) Self-intermediate function calculated at $T = 200$ K for different values of the wave vector k. Color dots are the calculated values and solid black lines are the fitted stretched exponential functions. The dots from top to bottom are for $k = 1, 5, 10, 15, \ldots, 100^{*}2\pi/l_x$. Red dots in the middle of the figure correspond to $k = 37^{*}2\pi/l_x$, which is the size of cages, and the solid red line corresponds to the stretched exponential function for that value of k.

nanoporous silica but their value of β is 0.60. This is due to the fact that their force field for water is short ranged. Khademi *et al.* have reported exactly the same value as us ($\beta \approx 3/7$) for water molecules confined in SiC nanotubes [12]. Their simulation includes long-range Coulomb interactions. These results suggest that stretched exponential decay of cage correlation function is a universal feature of nanoconfined liquids.

In 1982, Grassberger and Procaccia showed theoretically that particles diffusing in a medium with random traps would exhibit stretched exponential behavior. They derived the exact value of the exponent $\beta = d/(d+2)$, where d is the dimensionality of the system. (A brief summary of their derivation is given in the Supplemental Material.) In three dimensions, $\beta = 3/5$, which agrees with the MD simulation result of Shekhar *et al.* [9]. Phillips has shown that $\beta = d^{*}/(d^{*}+2)$, where $d^{*} = d/2$ is an effective spatial dimension in the presence of long-range Coulomb interaction [14]. He argues that particles diffuse not only in the real space but also in the subspace corresponding to polarization and that only real-space diffusion corresponds to the change of nearest neighbors. Our value of the exponent β agrees with this exact result because our force field for water includes long-range Coulomb interaction.

Stretched exponential decay has been reported in a variety of system, e.g., spin glasses [26], relaxation of a glass, and granular materials, to name a few. Welch *et al.* [30] measured strain relaxation in a glass sheet at room temperature over a period of 18 months and found stretched exponential behavior with $\beta = 3/7$, which agrees with the exact theoretical result.

We have also calculated the ISF $f(\boldsymbol{k}, t)$ to examine relaxation of nanoconfined water. The function $f(\boldsymbol{k}, t)$ is defined as [31]

$$f(\boldsymbol{k}, t) = \frac{1}{N}\sum_{j=1}^{N} \exp(-i\boldsymbol{k}\cdot(\boldsymbol{r}_j(t) - \boldsymbol{r}_j(0))), \qquad (3)$$

where $\boldsymbol{r}_j(0)$ denotes the position of the jth water molecule at time $t = 0$ and $\boldsymbol{r}_j(t)$ is the position of the same molecule at a later time t. This function provides information about the mean relaxation time of the system: ballistic motion at short timescales, cage motion at intermediate timescales, and molecules leaving cages (stretched exponential behavior) at long times. The ISF can be measured by neutron-scattering experiments. Chen and co-workers have reported measurements of ISF for D2O confined in pores of Vycor glass using neutron spin-echo spectrometers [32] and van Megen *et al.* have reported measurements of ISF for suspensions using dynamical light scattering [33].

Since our system is isotropic, we calculate $f(\boldsymbol{k}, t)$ for $\boldsymbol{k}$ along the x direction and fit the results to stretched exponential function $f(k, t) = \exp(-(t/\tau(k))^{\beta(k)})$ for a specific $k = 2\pi/\lambda$ value corresponding to the size of cages $\lambda = 3.14$ Å. The fitted parameters are $\beta(k) = 0.386$ and $\tau(k) = 0.67$ ns, and they both decrease as k increases. The decay of $f(k, t)$ is slower than exponential, which suggests the presence of dynamic heterogeneities in the system. $\beta(k)$ decreases from 0.9 for small k to 0.2 for large k and $\tau(k) \sim k^{-2}$ for small k (see the Supplemental Material). This is expected since the dynamical behavior is dominated by Brownian motion at large spatial and temporal scales. For large k, $\tau(k)$ decreases faster due to subdiffusive dynamics.

IV. CONCLUSION

In conclusion, MD simulations reveal significant changes in the structure and dynamics of water confined in nanometer-size pores of amorphous carbon. The local structure of LDW is different from that of HDW. The LDW molecules have complete first and second solvation shells, whereas only the first solvation shell of HDW is complete and the second solvation shell is broken. Confinement also has a dramatic effect on the dynamics of water molecules. Water molecules are not frozen even at temperatures as low as 200 K, although the self-diffusion coefficient drops sharply around 190 K. The cage correlation functions for nanoconfined water molecules at $T = 200$ and 250 K exhibit stretched exponential behavior with a universal exponent $\beta = 3/7$. This agrees not only with an exact theoretical prediction but also with experimental and simulation results for a variety of systems. Lastly, we have presented results on intermediate scattering function which also displays stretched exponential behavior. Our predictions regarding the universal value of β and the behavior of intermediate scattering function can be readily tested by neutron-scattering experiments.

ACKNOWLEDGMENTS

This work was supported by the U.S. Department of Energy, Office of Science, Basic Energy Sciences, under Award No. DE-SC0014607. The simulations were performed at the Argonne Leadership Computing Facility under the DOE INCITE program and at the Center for High Performance Computing of the University of Southern California.

[1] J. Xiao, D. Mei, X. Li, W. Xu, D. Wang, G. L. Graff, W. D. Bennett, Z. Nie, L. V. Saraf, I. A. Aksay, J. Liu, and J. G. Zhang, Nano Lett. **11**, 5071 (2011).

[2] Z. Zhao, E. F. Wang, H. Yan, Y. Kono, B. Wen, L. Bai, F. Shi, J. Zhang, C. Kenney-Benson, C. Park, Y. Wang, and G. Shen, Nat. Commun. **6**, 6212 (2015).

[3] A. E. Aliev, J. Oh, M. E. Kozlov, A. A. Kuznetsov, S. Fang, A. F. Fonseca, R. Ovalle, M. D. Lima, M. H. Haque, Y. N. Gartstein, M. Zhang, A. A. Zakhidov, and R. H. Baughman, Science **323**, 1575 (2009).

[4] H.-L. Jiang, B. Liu, Y.-Q. Lan, K. Kuratani, T. Akita, H. Shioyama, F. Zong, and Q. Xu, J. Am. Chem. Soc. **133**, 11854 (2011).

[5] E. Lam and J. H. T. Luong, ACS Catal. **4**, 3393 (2014).

[6] M. Li, F. Xu, H. Li, and Y. Wang, Catal. Sci. Technol. **6**, 3670 (2016).

[7] K. V. Agrawal, S. Shimizu, L. W. Drahushuk, D. Kilcoyne, and M. S. Strano, Nat. Nanotechnol. **12**, 267 (2017).

[8] K. Koga, G. T. Gao, H. Tanaka, and X. C. Zeng, Nature(London) **412**, 802 (2001).

[9] A. Shekhar, R. K. Kalia, A. Nakano, P. Vashishta, C. K. Alm, and A. Malthe-Sørenssen, Appl. Phys. Lett. **105**, 161907 (2014).

[10] J. A. Sellberg, C. Huang, T. A. McQueen, N. D. Loh, H. Laksmono, D. Schlesinger, R. G. Sierra, D. Nordlund, C. Y. Hampton, D. Starodub, D. P. Deponte, M. Beye, C. Chen, A. V. Martin, A. Barty, K. T. Wikfeldt, T. M. Weiss, C. Caronna, J. Feldkamp, L. B. Skinner, M. M. Seibert, M. Messerschmidt, G. J. Williams, S. Boutet, L. G. M. Pettersson, M. J. Bogan, and A. Nilsson, Nature (London) **510**, 381 (2014).

[11] P. Grassberger, J. Chem. Phys. **77**, 6281 (1982).

[12] M. Khademi, R. K. Kalia, and M. Sahimi, Phys. Rev. E **92**, 030301(R) (2015).

[13] J. C. Phillips, J. Non. Cryst. Solids **357**, 3853 (2011).

[14] J. C. Phillips, Rep. Prog. Phys. **59**, 1133 (1996).

[15] K. Nomura, R. K. Kalia, Y. Li, A. Nakano, P. Rajak, C. Sheng, K. Shimamura, F. Shimojo, and P. Vashishta, Sci. Rep. **6**, 1 (2016).

[16] A. K. Soper and M. A. Ricci, Phys. Rev. Lett. **84**, 2881 (2000).

[17] A. C. T. Van Duin, S. Dasgupta, F. Lorant, and W. A. Goddard, J. Phys. Chem. A **105**, 9396 (2001).

[18] T. P. Senftle, S. Hong, M. M. Islam, S. B. Kylasa, Y. Zheng, Y. K. Shin, C. Junkermeier, R. Engel-Herbert, M. J. Janik, H. M. Aktulga, T. Verstraelen, A. Grama, and A. C. T. van Duin, npj Comput. Mater. **2**, 15011 (2016).

[19] D. A. Newsome, D. Sengupta, H. Foroutan, M. F. Russo, and A. C. T. van Duin, J. Phys. Chem. C **116**, 16111 (2012).

[20] S. J. Stuart, A. B. Tutein, and J. A. Harrison, J. Chem. Phys. **112**, 6472 (2000).

[21] J. L. F. Abascal and C. Vega, J. Chem. Phys. **123**, 234505 (2005).

[22] J. Włoch, A. P. Terzyk, and P. Kowalczyk, Chem. Phys. Lett. **674**, 98 (2017).

[23] A. I. Aria, P. R. Kidambi, R. S. Weatherup, L. Xiao, J. A. Williams, and S. Hofmann, J. Phys. Chem. C **120**, 2215 (2016).

[24] S. Plimpton, J. Comput. Phys. **117**, 1 (1995).

[25] See Supplemental Material at http://link.aps.org/supplemental/10.1103/PhysRevMaterials.2.115605 for a detailed explanation of cage-correlation function, fitting of self-intermediate scattering functions, hydrogen-bond network, formation of nanoporous carbon, and self-diffusion coefficient of bulk water.

[26] A. T. Ogielski, Phys. Rev. B **32**, 7384 (1985).

[27] T. M. Truskett, S. Torquato, and P. G. Debenedetti, Phys. Rev. E **62**, 993 (2000).

[28] E. Rabani, J. D. Gezelter, and B. J. Berne, Phys. Rev. Lett. **82**, 3649 (1999).

[29] H. Childs, E. Brugger, B. Whitlock, J. Meredith, S. Ahern, D. Pugmire, K. Biagas, M. Miller, C. Harrison, G. H. Weber, H. Krishnan, T. Fogal, A. Sanderson, C. Garth, E. W. Bethel, D. Camp, O. Rübel, M. Durant, J. M. Favre, and P. Navrátil, in *High Performance Visualization–Enabling Extreme-Scale Scientific Insight* (2012), pp. 357–372.

[30] R. C. Welch, J. R. Smith, M. Potuzak, X. Guo, B. F. Bowden, T. J. Kiczenski, D. C. Allan, E. A. King, A. J. Ellison, and J. C. Mauro, Phys. Rev. Lett. **110**, 265901 (2013).

[31] J.-P. Hansen and I. R. McDonald, *Theory of Simple Liquids*, 3rd ed. (Academic Press, 2006), p. 198.

[32] M. C. Bellissent-Funel, S. Longeville, J. M. Zanotti, and S. H. Chen, Phys. Rev. Lett. **85**, 3644 (2000).

[33] W. van Megen, T. C. Mortensen, S. R. Williams, and J. Müller, Phys. Rev. E **58**, 6073 (1998).

[34] A. Stukowski and K. Albe, Model. Simul. Mater. Sci. Eng. **18**, 085001 (2010).